Journal of Physics B: Atomic, Molecular and Optical Physics

PAPER

Atomic dynamic interference in intense linearly and circularly polarized XUV pulses

To cite this article: Jintai Liang *et al* 2020 *J. Phys. B: At. Mol. Opt. Phys.* **53** 095601

IOP Publishing Journal of Physics B: Atomic, Molecular and Optical Physics
J. Phys. B: At. Mol. Opt. Phys. **53** (2020) 095601 (10pp) https://doi.org/10.1088/1361-6455/ab7527

Atomic dynamic interference in intense linearly and circularly polarized XUV pulses

Jintai Liang[1], Wei-Chao Jiang[2,4], Shun Wang[2], Min Li[1], Yueming Zhou[1,4] and Peixiang Lu[1,3]

[1] School of Physics and Wuhan National Laboratory for Optoelectronics, Huazhong University of Science and Technology, Wuhan 430074, People's Republic of China
[2] College of Physics and Optoelectronic Engineering, Shenzhen University, Shenzhen 518060, People's Republic of China
[3] Laboratory of Optical Information Technology, Wuhan Institute of Technology, Wuhan 430205, People's Republic of China

E-mail: jiang.wei.chao@szu.edu.cn and zhouymhust@hust.edu.cn

Received 11 November 2019, revised 1 February 2020
Accepted for publication 11 February 2020
Published 30 March 2020

Abstract

By numerically solving the three-dimensional time-dependent Schrödinger equation, we theoretically investigate the dynamic interference of the hydrogen atom in intense arbitrarily polarized high-frequency XUV pulses with and without the non-dipole correction included. Our results show a clear shift of the dynamic-interference peaks in the photoelectron spectra from the linearly and circularly polarized XUV pulses, which can be attributed to the different AC Stark shifts of the ground state. The non-dipole correction for the electron–light interaction produces a similar peak shift along the propagation direction in the photoelectron momentum spectra for the linear and circular pulses. But no obvious non-dipole effect for the AC Stark shift of the ground state is identified for the light pulse with intensity around 10^{19} W cm^{-2}.

Keywords: dynamic interference, AC Stark effect, non-dipole effect

(Some figures may appear in colour only in the online journal)

1. Introduction

The general field of laser–matter interaction is characterized by impressive progress in light-source technology. Light sources with intense intensity in the XUV frequency regions are being rapidly developed [1–6]. For instance, free-electron lasers promise to provide laser pulses with intensity above 10^{20} W cm^{-2}. In such high-intensity laser pulses, highly nonlinear interactions between the laser pulses and matter are expected in the XUV frequency region. One of the remarkable and counterintuitive phenomena is atomic stabilization, which has been theoretically [7–13] and experimentally [14–17] investigated for decades. Moreover, the nonlinear interactions at high photon energy exceeding the ionization energy can produce interference effects like dynamic interference [18–29].

For a low-intensity XUV pulse, according to Einstein's photoelectric law, a single peak at $E = \omega - I_p$ in the energy spectrum of the photoelectrons is expected. With the increase in the peak intensity of the laser pulse, the single peak can be shifted or even gradually evolve into multi-peak structures. This modulation of the spectrum originates from the dynamic interference mechanism. The principles and conditions to observe such an interference effect have been explained in previous works [26, 30]. In the presence of the intense laser pulse, the binding potential of the system can be modified by the AC Stark effect [31–35]. The electron wave packets, which are ejected on the rising and falling edges of the laser pulse, respectively, and reach the same final energy when the instantaneous AC Stark shifts of the ionization potential coincide at two different times, can interfere with each other and produce the interference structures in the energy spectrum of the photoelectrons. Similar interferences have also been predicted earlier and observed in the low-frequency multi-photon region [36–42]. Moreover, the atomic stabilization can be important in the intense laser pulses, and the onset of atomic stabilization is closely related to the appearance of the

[4] Authors to whom any correspondence should be addressed.

dynamic interference [30]. Furthermore, the non-dipole correction plays a non-negligible role in high laser intensities at large photon energies. For instance, it has been pointed out that the non-dipole effect may weaken the atomic stabilization [8, 43–49]. Very recently, the non-dipole effect of the dynamic interference has been theoretically investigated for a linearly polarized laser pulse [50]. Furthermore, the dynamic interference for the double ionization of helium has been investigated [51]. Most of the previous investigations on the dynamic interference mainly focused on linearly polarized pulses. The existence of dynamic interference in circularly polarized pulses has been confirmed in a previous theoretical study on H^- [20]. Peak shift in the photoelectron energy spectra for a linearly polarized pulse and a circularly polarized laser pulse was implicated in the calculation results, but no detailed explanation for the peak shift was given. Moreover, the non-dipole effect on the dynamic interference for non-linearly polarized pulses has not been investigated as far as we know.

In this work, we study the dynamic interference of the H atom in intense linearly and circularly polarized high-frequency XUV laser pulses by numerically solving the three-dimensional (3D) time-dependent Schrödinger equation (TDSE). At low intensity, no difference is identified in the photoelectron energy spectra for linearly and circularly polarized laser pulses. However, obvious dynamic-interference shifts can be observed in the energy spectra for laser pulses with different polarizations at high intensities. This shift increases as the photon energy of the laser pulse decreases. By extracting the instantaneous AC Stark shift of the initial state from the TDSE calculation, we find that this shift originates from the different AC Stark shifts of the ground state in circularly and linearly polarized pulses. The second-order perturbation theory and zero-order high-frequency Floquet theory (HFFT) are invalid for describing the polarization dependence of the AC Stark shift in such intense laser pulses. A polynomial is raised to fit the energy shift of the ground state in differently polarized pulses. We verify that the non-dipole effect produces a similar peak shift along the propagation direction in the photoelectron momentum distributions (PEMDs) for the linear and circular laser pulses, which originates from the fact that the AC Stark shift of the continuous states are dependent on the ejection angle after non-dipole correction is included. No obvious non-dipole effect on the AC Stark shift of the ground state is identified for the laser parameters considered in this work.

This paper is organized as follows. In section 2, we introduce our method for numerically solving the 3D TDSE. Then, we analyze the dynamic interference in the differently polarized pulses within dipole approximation in section 3.1. In section 3.2, we investigate the non-dipole effect on dynamic interference in circularly polarized pulses. Section. 4 provides a brief summary.

2. Theoretical methods

We investigate the dynamic interference by numerically solving the 3D TDSE. The TDSE for the H atom is (atomic units are used unless otherwise stated)

$$i\frac{\partial\Psi(\mathbf{r},t)}{\partial t}=H\Psi(\mathbf{r},t), \tag{1}$$

where the Hamiltonian in the velocity gauge is given by

$$H=\frac{[\mathbf{p}+A(r,t)]^2}{2}+V(\mathbf{r}), \tag{2}$$

where $V(\mathbf{r})=-1/r$ is the attractive Coulomb potential of the H atom.

In the dipole approximation, the vector potential $\mathbf{A}(t)$ of the laser pulse is space-independent, and the Hamiltonian in the dipole approximation is written as

$$H_{\mathrm{D}}=-\frac{1}{2}\nabla^2+V(r)-i\mathbf{A}(t)\cdot\nabla. \tag{3}$$

Here, we have omitted the term $\mathbf{A}^2(\mathbf{r},t)/2$, which only contributes a global phase $\exp[i\int_{-\infty}^{t}\mathbf{A}^2(\mathbf{r},\tau)/2d\tau]$ of the wave function and can be canceled by gauge transform. The global phase does not change any physical observations, but it indeed induces the gauge dependence of the AC Stark shift which has been discussed in the previous work [26].

When the lowest-order non-dipole correction is considered, the vector potential $\mathbf{A}(\mathbf{r},t)$ is both time- and space-dependent, and it is expressed as

$$\mathbf{A}(\mathbf{r},t)=\mathbf{A}(t)+\frac{1}{c}(\mathbf{k}\cdot\mathbf{r})\mathbf{F}(t). \tag{4}$$

Here, $\mathbf{A}(t)$ and $\mathbf{F}(t)$ are the usually adopted vector potential and electric field of the laser pulse in the dipole approximation, respectively, where $\mathbf{k}$ is the unit vector in the direction of the laser propagation and c is the vacuum light speed. Inserting equation (4) into equation (2), we express the lowest-order corrected non-dipole Hamiltonian as

$$\begin{aligned}H_{\mathrm{ND}}=&-\frac{1}{2}\nabla^2+V(r)-i\mathbf{A}(t)\cdot\nabla\\&+\frac{1}{c}(\mathbf{k}\cdot\mathbf{r})[\mathbf{A}(t)\cdot\mathbf{F}(t)]-i\frac{1}{c}(\mathbf{k}\cdot\mathbf{r})\mathbf{F}(t)\cdot\nabla.\end{aligned} \tag{5}$$

In our simulation, the laser pulse propagates along the positive y axis and is polarized in the x-z plane. The vector potential $\mathbf{A}(t)$ of the laser pulse is written as

$$\begin{aligned}A_z(t)&=A_0f(t)\sin(\omega t)\frac{1}{\sqrt{1+\eta^2}},\\A_x(t)&=-A_0f(t)\cos(\omega t)\frac{\eta}{\sqrt{1+\eta^2}},\end{aligned} \tag{6}$$

where A_0 is the amplitude of the vector potential, η is the ellipticity with $\eta=0$ and $\eta=1$ representing the linearly and circularly polarized laser pulses, respectively, and $f(t)$ is the envelope of the laser pulse, which is written as

$$f(t)=\exp\left[-2\ln 2\left(\frac{t}{\tau}\right)^2\right], \tag{7}$$

where τ is the full width at half maximum (FWHM) of the laser pulse.

In our simulation, the TDSE in equation (1) is solved in the spherical coordinates, in which the wave function $\Psi(\mathbf{r},t)$

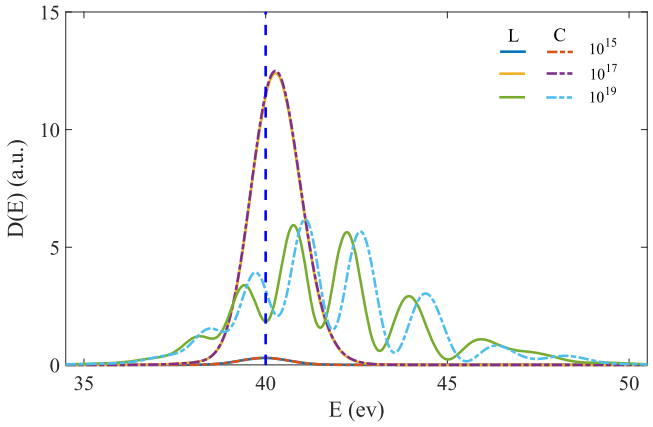

Figure 1. The photoelectron energy spectra for the H atom ionized by the laser pulses with different intensities. The solid and dot-dashed lines are the results for the linearly and circularly polarized laser pulses, respectively. The intensities are shown in the legend (in W cm^{-2}). The vertical dashed line marks the energy position at $E = \omega - I_p$. The photon energy and FWHM of the laser pulses are 53.6 eV and 15 cycles, respectively.

is expanded by spherical harmonics $|lm\rangle$,

$$|\Psi(\mathbf{r}, t)\rangle = \sum_{l,m} \frac{R_{lm}(r, t)}{r}|lm\rangle, \tag{8}$$

where $R_{lm}(r, t)$ is the radial part of the wave function. This radial wave function is discretized by a finite-element discrete variable representation method [52]. The matrix elements of the Hamiltonian in the representation of spherical harmonics are given in the appendix. The time propagation of the TDSE is calculated by the split-Lanczos method [53] with the time step fixed at $\Delta t = 0.01$ a.u. The initial wave function is prepared by the imaginary-time propagation. The ionization amplitude is extracted from the final wave function by projecting it to the scattering state $|\Psi_{\mathbf{p}}(\mathbf{r})\rangle$,

$$M(\mathbf{p}) = \langle\Psi_{\mathbf{p}}(\mathbf{r})|\Psi(\mathbf{r}, t)\rangle. \tag{9}$$

Then, the energy spectrum of the photoelectron is given by

$$D(E) = \int\int |M(\mathbf{p})|^2 |\mathbf{p}|\, sin\theta d\theta d\phi, \tag{10}$$

where θ and ϕ are the polar and azimuthal angle of the photoelectron in the spherical coordinate frame, respectively.

3. Results and discussion

3.1. Dynamic interference in dipole approximation

Figure 1 shows the photoelectron energy spectra for a H atom ionized by the laser pulses with different intensities. The results are calculated in dipole approximation. Here, the frequency and FWHM of the laser pulses are $\omega = 53.6$ eV and $\tau = 15$ cycles, and we consider both the linearly and circularly polarized laser pulses. For the lowest intensity, $I_0 = 1 \times 10^{15}$ W cm^{-2}, the spectrum shows a single peak locating at $E = \omega - I_p = 40$ eV. As the intensity increases to $I_0 = 1 \times 10^{17}$ W cm^{-2}, the peak becomes stronger due to the higher ionization probability, and the position of the peak shifts towards higher energy. This shift originates from the AC Stark shift of the ground state [28]. For these intensities, the spectra for the linear and circular laser pulses are the same. When the intensity increases to $I_0 = 1 \times 10^{19}$ W cm^{-2}, modulation appears on the energy spectra. This modulation originates from the dynamic interference, and it has been extensively studied previously [18–28, 30]. The interesting result here is that the dynamic interference fringes in the circular laser pulse shift towards the high energy relative to the linear case. Such a shift has also been observed in a previous study for H^- [20], but without detailed explanation.

As demonstrated previously [18–21], the dynamic interference pattern is determined by the AC Stark shift of the ground state. To understand the shift of the interference in the linear and circular laser field, we extract the AC Stark shift of the ground state in the TDSE calculation. The exact expression for the probability amplitude $a_E(t)$ for the populating of the continuum state with energy E can be written as

$$a_E(t) = -ie^{-iEt}\sum_j \mathbf{p}_{Ej} \cdot \int_{-\infty}^{t} \mathbf{A}(t')a_j(t')e^{iEt'}dt', \tag{11}$$

where $a_j(t')$ is the amplitude of the eigenstate $|\Psi_j\rangle$ of the field-free Hamiltonian, and $\mathbf{p}_{Ej} = \langle\Psi_E|\mathbf{p}|\Psi_j\rangle$ is the transition matrix element from $|\Psi_j\rangle$ to $|\Psi_E\rangle$. Since the photon energy of the laser pulse is much higher than the binding potential of the ground state of the H atom and the narrow spectrum width due to the ~fs scale pulse duration, the transition from other channels, except the ground state ($j = 0$), can be neglected. Then, equation (11) is reduced to

$$a_E(t) = -ie^{-iEt}\mathbf{p}_{E0} \cdot \int_{-\infty}^{t} \mathbf{A}(t')a_0(t')e^{iEt'}dt'. \tag{12}$$

Obviously, the probability amplitude $a_E(t)$ only depends on $a_0(t)$ for a certain laser pulse. The validity of equation (12) has been checked in [30]. In our TDSE calculation, $a_0(t)$ can be obtained by projecting $|\Psi(t)\rangle$ to $|\Psi_0\rangle$,

$$a_0(t) = \langle\Psi_0|\Psi(t)\rangle = g(t)e^{-i\phi(t)}. \tag{13}$$

Here, $g(t)$ and $\phi(t)$ are the modulus and phase of the amplitude, respectively. Then, the AC Stark shift of the ground state in the TDSE calculation can be extracted by

$$E_0(t) = \frac{d\phi(t)}{dt}. \tag{14}$$

Figure 2 displays this time-dependent energy of the ground state for different intensities. The parameters of the laser pulses are the same as those in figure 1. Note that the energy shift extracted from equation (14) depends on the instantaneous strength of the electric field. For the circularly polarized pulse, the strength of the electric field follows the envelope of the laser pulse, and there are no oscillations in the time-dependent energy shift, as shown by the red line in the inset of figure 2. On the contrary, in the linear case, $E_0(t)$ oscillates fast at twice the frequency of the laser pulse, as shown by the blue line in the inset of figure 2. We apply a mean filter method to smooth the oscillating energy [30]. The obtained cycle-averaged energies of the ground state are shown by the solid line in figure 2. For the lowest intensity, $I_0 = 1 \times$

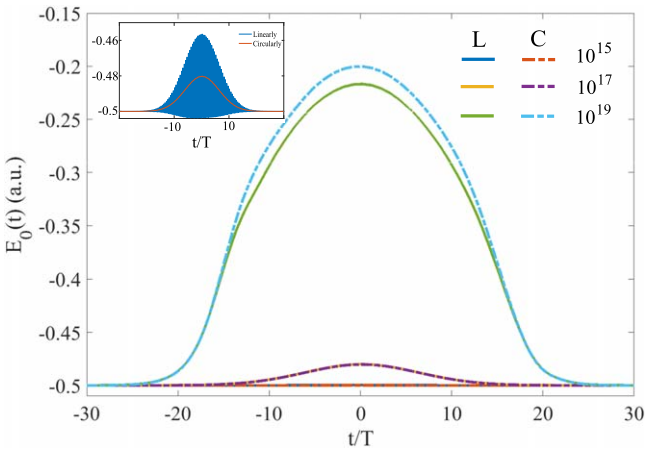

Figure 2. The time-dependent energy $E_0(t)$ of the ground state. T is the period of the laser pulse. The laser parameters are the same as those in figure 1. The inset shows the original data exacted from the TDSE calculation. The blue and red lines are the results for the linearly and circularly polarized pulses, respectively. The results after application of a mean filter tracing the envelope of the pulse are shown in the figure. The solid and dashed lines are the results for the linear and circular polarization laser pulses, respectively. The intensities are shown in the legend (in W cm^{-2}).

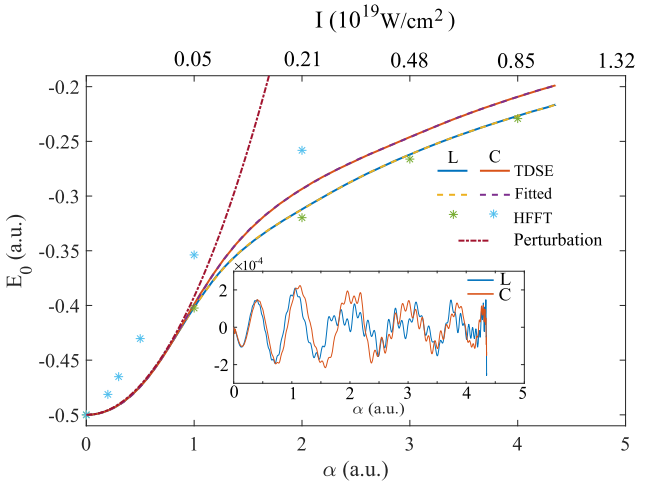

Figure 3. Energy of the ground state of the H atom as a function of the excursion amplitude $\alpha = F(t)/\omega^2$ at $\omega = 53.6$ eV. The solid and dashed lines are the results extracted from the TDSE and fitting formula of equation (20), respectively. The dot-solid line and the symbols are the results from the second-order perturbation theory [26] and zero-order HFFT [9, 56] for the AC Stark shifts. The polarization of the laser pulse is shown in the legend. The inset displays the fitting error of the formula.

10^{15} W cm^{-2}, the AC Stark shift of the ground state can be neglected. Therefore, the photoelectron's energy spectrum is a single peak locating at $E = \omega - I_p = 40$ eV. For $I_0 = 1 \times 10^{17}$ W cm^{-2}, the energy shift of the ground state is significant, and the peaks of the photoelectron energy spectra in figure 1 shift towards the high energy region. At this laser intensity, the AC Stark shifts of the ground state are nearly the same for the linearly and circularly polarized pulses, and thus their energy spectra are the same. At $I_0 = 1 \times 10^{19}$ W cm^{-2}, the AC Stark shift is much larger than the lower intensities, and the shift difference between the linear and circular laser field is obvious. The dynamic interference fringes shown in figure 1 originate from this huge energy shift of the ground state. The phase difference $\Delta\Phi(E)$ determining the dynamic interference structure is given by [30]

$$\Delta\Phi(E) = \int_{t_1(E)}^{t_2(E)} [E_0(t) - E_0(t_1)]dt + \frac{\pi}{2}, \tag{15}$$

where t_i ($i = 1, 2$) are the solutions of $E = \omega + E_0(t)$. Note that the phase contribution $\pi/2$ in equation (15) is due to the caustics $\frac{d}{dt}E_0(t) < 0$ [30]. On account of the distinct difference in energy shift of the ground state in linearly and circularly polarized laser pulses, the phase $\Delta\Phi(E)$ in equation (15) is different for these two types of polarized laser pulses. Therefore, the obvious dynamic interference shift in circularly polarized pulses relative to the linear case originates from the different AC Stark shift of the ground state. It indicates that the difference in the AC Stark shifts for the ground state in circularly and linearly polarized pulses can be directly observed by these experimentally measurable dynamic interference fringes.

The physical picture of these different energy shifts in circular and linear pulses can be qualitatively understood in the Kramers–Henneberger (K-H) frame. By the unitary transition operator $U = \exp[i\boldsymbol{\alpha}(t) \cdot \mathbf{p}]$, the Hamiltonian in equation (2) can be transformed to

$$H_{\mathrm{KH}} = \frac{1}{2}\mathbf{p}^2 + V[\mathbf{r} + \boldsymbol{\alpha}(t)], \tag{16}$$

where $\boldsymbol{\alpha}(t) = \mathbf{F}(t)/\omega^2$ is the excursion amplitude. For the linearly polarized pulses, the dressed potential of the H atom in the laser field is similar to the separated atom limit of a homo-nuclear diatomic molecule centered around the end-points, $\pm\alpha_0 = \pm F_0/\omega^2$ [54]. Here, F_0 is the amplitude of the electric field, $F(t)$. For circularly polarized pulses, the dressed potential is toroidal shaped with a radius of $\alpha_0 = F_0/\omega^2$ [55]. These different laser-induced potentials lead to the different AC Stark shifts in linearly and circularly polarized pulses.

We compare the energy shifts extracted from the TDSE calculation and other models in figure 3. The solid lines are the results extracted from the TDSE calculation at $\omega = 53.6$ eV and $\tau = 40$ cycles. The energy shifts for differently polarized pulses are the same in the low α region. The difference appears when $\alpha > 1$. The dot-dashed line is the result from the second-order perturbation theory [26]. In this approximation, the time-dependent energy of the ground state is

$$E_0(t) = \delta E_p(t) - I_p, \tag{17}$$

where $E_p(t) = F(t)^2/\omega^2$ is the ponderomotive energy, and $I_p = 0.5$ a.u. is the binding energy of the ground state for the H atom. The coefficient δ is [26]

$$\delta \propto \omega^{-2}. \tag{18}$$

Thus, we have

$$E_0(t) + I_p \propto \frac{F(t)^2}{\omega^4} = \alpha^2. \tag{19}$$

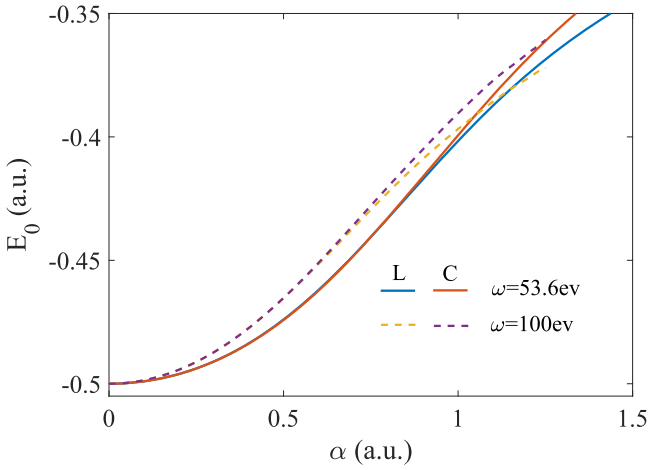

Figure 4. Energy of the ground state of the H atom as functions of α at $\omega = 53.6$ eV(solid lines) and $\omega = 100$ eV (dashed lines). The polarization of the laser pulses is shown in the legend.

At small α, the result of the second-order perturbation theory agrees well with the TDSE result. Note that the AC Stark shift of the ground state is positive due to the fact that the frequency is much larger than the binding potential of the ground state, even in the perturbation region. As α increases (where the laser intensity increases), it deviates significantly from the TDSE results. This is due to the fact that the high-order perturbation terms cannot be neglected in this intense laser pulse.

Figure 3 also shows the results obtained from the zero-order HFFT [9, 56]. The prediction of the linearly polarized pulse by the zero-order HFFT coincides with the TDSE results. However, for the circularly polarized pulse, the zero-order HFFT breaks down. Moreover, in the zero-order HFFT, the energy shift of the ground state depends on the photon energy and laser intensity through α. For a fixed α, the energy shifts are independent of the photon energy and laser intensity. Here, we show the energy of the ground state as a function of α for $\omega = 53.6$ eV (solid lines) and $\omega = 100$ eV (dashed lines) extracted from the TDSE calculation in figure 4. Apparently, the energy shift of the ground state depends on the photon energy of the laser field. The energy shifts at $\omega = 100$ eV are significantly higher than at $\omega = 53.6$ eV. Our numerical results show the same tendency as the accurate Floquet calculations [57]. It indicates that the zero-order HFFT is not suitable in such an intense laser pulse. This frequency-dependent energy shift explains why the zero-order HFFT cannot fully describe the dynamic interference structures in the previous work (see figure 8 in [20]).

We use a polynomial

$$E_0(t) = I_p + \sum_{n=2}^{n=13} a_n \alpha^n, \tag{20}$$

to fit the AC Stark shift as the function of α for the ground state. For the ground state of an atom, the first-order effect is zero. Thus, the fitting formula is from the α^2 term. Our results show that the polynomial can give a relatively exact result when $n = 13$, as shown by the dashed lines in figure 3. The inset shows the fitting error as the function of α. Our fitting formula can give relatively exact results in the intensity region at $[0,\ 1.5 \times 10^{19}]$ W cm^{-2}, with errors below 2×10^{-4}. Table 1 displays the coefficients of the fitting formula.

To test the feasibility of our fitting formula, the time-dependent energy shifts for different pulse duration and laser intensity are calculated. The results are displayed in figure 5. The laser intensity is 1×10^{18} W cm^{-2}, and the pulse durations for figures 5(a) and (b) are $\tau = 30$ cycles and $\tau = 7$ cycles, respectively. The solid lines are the results exacted from the TDSE, and the dashed lines are calculated by the fitting formula. Obviously, our fitting formula can describe the time-dependent energy of the ground state rather well.

In principle, the different energy shifts for circularly and linearly polarized pulses can be observed from the peak position of the single peak structures in the photoelectron energy spectrum. However, due to the atomic stabilization, the maximal probability of ionization does not occur at the peak of the laser pulses where the energy shift difference between the circular and linear laser pulses of the ground state is maximum. It means that the different AC Stark shift of the ground state is not easy to directly observe from the single peak structure. To observe this energy shift difference, an experimentally available dynamic interference structure is a very promising candidate. The previous work has demonstrated that the dynamic interference is more evident for a shorter duration laser pulse and strong enough intensity [30]. To show the differences in the interference structures in differently polarized laser pulses more clearly, the energy spectra for a shorter pulse duration and different photon energies are calculated. The results are shown in figure 6. The FWHM is $\tau = 7$ cycles, and the photon energy for figures 6(a)–(d) are 100 eV, 53.6 eV, 40.8 eV and 26 eV, respectively. According to figure 3, the difference in the energy shift between linear and circular laser pulses is more obvious at larger α (smaller photon energy). Therefore, the interference fringe's shift in the circular pulse relative to the linear case is more evident as the photon energy decreases. This fringe's shift in lower photon energy is advantageous for observing the energy shift difference for differently polarized laser pulses experimentally.

3.2. Non-dipole effect in dynamic interference

In the very intense laser field, the non-dipole effect can be important. In the low frequency, the non-dipole correction induces a contrary momentum shift for linearly and circularly polarized pulses due to the recollision in the linearly polarized pulse [58–63]. Very recently, the non-dipole effect on dynamic interference in linearly polarized pulses for high photon energy has been investigated [50]. The momentum shift still exists, and it mainly comes from the non-dipole correction of the Volkov phase. Here, we examine the non-dipole effect on the circular laser pulse. Figure 7 shows the PEMDs in the p_z-p_y plane ($p_x = 0$) for $p_y > 0$. The intensity of the laser pulse is 1×10^{19} W cm^{-2}, and the photon energy is $\omega = 53.6$ eV with pulse duration $\tau = 7$ cycles. The upper panels display the results in the dipole approximation, and the

Table 1. The coefficients in equation (20).

Coefficient	Linear	Circular	Coefficient	Linear	Circular
a_2	0.122922	0.118 041	a_8	−0.158248	−0.327789
a_3	−0.235654	−0.172880	a_9	0.092 061 7	0.140 407
a_4	0.780403	0.498 736	a_{10}	−0.0269380	−0.0361517
a_5	−1.03103	−0.464452	a_{11}	$4.508\,638 \times 10^{-3}$	$5.638\,64 \times 10^{-3}$
a_6	0.548 375	−0.0610084	a_{12}	-4.12126×10^{-4}	-4.92937×10^{-4}
a_7	$2.150\,83 \times 10^{-3}$	0.400 532	a_{13}	$1.602\,99 \times 10^{-5}$	$1.859\,34 \times 10^{-5}$

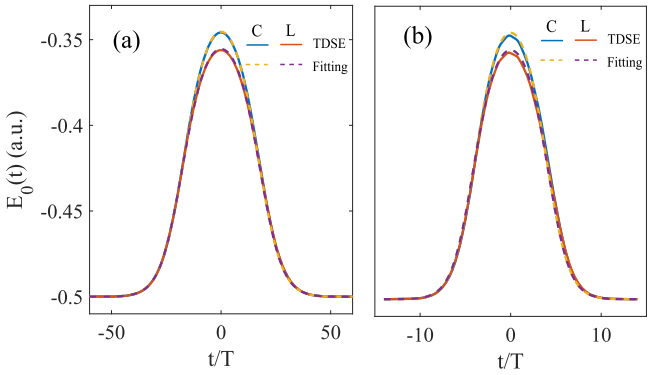

Figure 5. The time-dependent energy $E_0(t)$ of the ground state. The solid and dashed lines are the results extracted from the TDSE and calculated by the fitting formula of equation (20). The laser intensity is 1×10^{18} W cm^{-2}, and the pulse durations for (a) and (b) are $\tau = 30$ cycles and $\tau = 7$ cycles, respectively. The polarization of the laser pulses is shown in the legend.

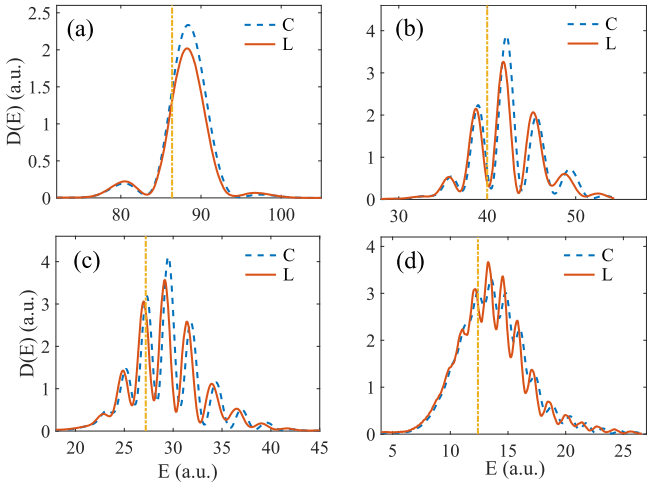

Figure 6. The photoelectron energy spectrum for the ground state of the H atom at four different photon energies: (a) $\omega = 100$ eV, (b) $\omega = 53.6$ eV, (c) $\omega = 40.8$ eV and (d) $\omega = 26$ eV. The pulse duration and the laser intensity are $\tau = 7$ cycles and $I_0 = 1 \times 10^{19}$ W cm^{-2}. The dashed and solid lines are the results for the circularly and linearly polarized pulses, respectively. The yellow dot-solid lines mark the energy position at $E = \omega - I_p$.

bottom panels are the results with non-dipole correction. The left (figures 7(a) and (c)) and right (figures 7(b) and (d)) panels are the results for the circularly and linearly polarized pulses, respectively. In the dipole approximation, the interference fringes do not change with θ. Whereas, when the non-dipole effect is considered, the momentum for the maxima of

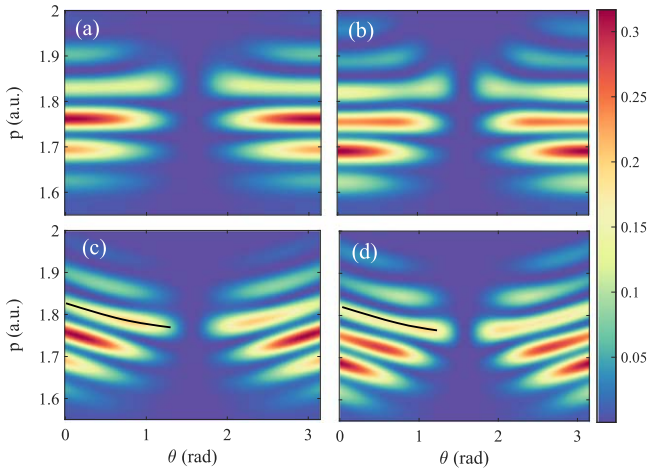

Figure 7. The PEMDs in the p_z-p_y plane ($p_x = 0$) for $p_y > 0$. The intensity of the laser pulse is 1×10^{19} W cm^{-2} with photon energy at $\omega = 53.6$ eV and $\tau = 7T$. Here, θ and p are the polar angle and photoelectron momentum, respectively. The upper panels are the results for the dipole TDSE calculation and the bottom panels are the results for the non-dipole TDSE calculation. The left ((a) and (c)) and right ((b) and (d)) panels are the results for the circularly and linearly polarized pulses, respectively.

the interference structures decreases with θ. This observation coincides with a previous report on the momentum shift towards the opposite direction of the laser propagation due to the non-dipole effect [50]. In figure 8, we show a scheme to illustrate this momentum shift. In the dipole approximation, the momenta for the maxima of the dynamic interference distribute on the ring centered at the origin point o, as shown by the solid line. Thus, the momentum for the maxima of the dynamic interference does not change with θ. With non-dipole correction, the center of the ring shifts Δp towards the opposite direction of the laser propagation to o', as shown by the dot-dashed line. Therefore, the momentum for the maxima of the dynamic interference decreases with θ. In this simple geometry, the relation between the momentum and θ with non-dipole correction can be given by

$$p_0^2 = p^2 + \Delta p^2 - 2\Delta p \cdot p \sin\theta, \tag{21}$$

where p_0 is the radius of the ring structure, and p is the momentum for the maxima of the interference fringes. The symbols in figure 9(a) show the maxima of the interference fringe in figures 7(c) and (d) (the black solid lines). We fit these data with equation (21) to obtain the radius p_0 of the interference ring and the momentum shift Δp due to the

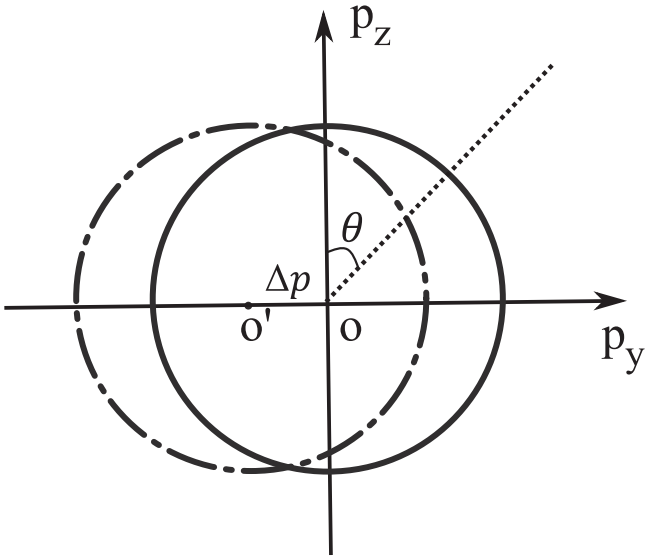

Figure 8. A schematic illustration of the non-dipole effect of the PEMD. The solid circle centered on o represents the momentum distribution with dipole approximation, and the dot-solid circle centered on o' is the momentum distribution with non-dipole correction. Here, Δp is the momentum shift due to the non-dipole effect, and θ is the angle between the photoelectron emission direction and the z axis.

non-dipole effect. The results are

$$\Delta p = 0.059(\pm 0.005) \quad p_0 = 1.827(\pm 0.001) \quad \text{Circular},$$
$$\Delta p = 0.054(\pm 0.005) \quad p_0 = 1.816(\pm 0.001) \quad \text{Linear}. \tag{22}$$

The obtained momentum shifts Δp are the same for the circularly and linearly polarized pulses in the confidence interval, and they coincide with the results in the previous work [50]. It indicates that the shifts in PEMDs caused by the non-dipole effect are similar in the differently polarized pulses.

For the radius p_0, the data in the circular pulse is a little larger than the case in the linear pulse. This indicates that the dynamic interference shift between the circular and linear laser pulses still exists when the non-dipole effect is considered. We extract the time-dependent energy of the ground state from the TDSE calculation, and the results are shown in figure 9(b). The dashed and solid lines are the results obtained with and without non-dipole correction, respectively. Apparently, the non-dipole interaction does not change the energy of the ground state for both the linear and circular laser pulses.

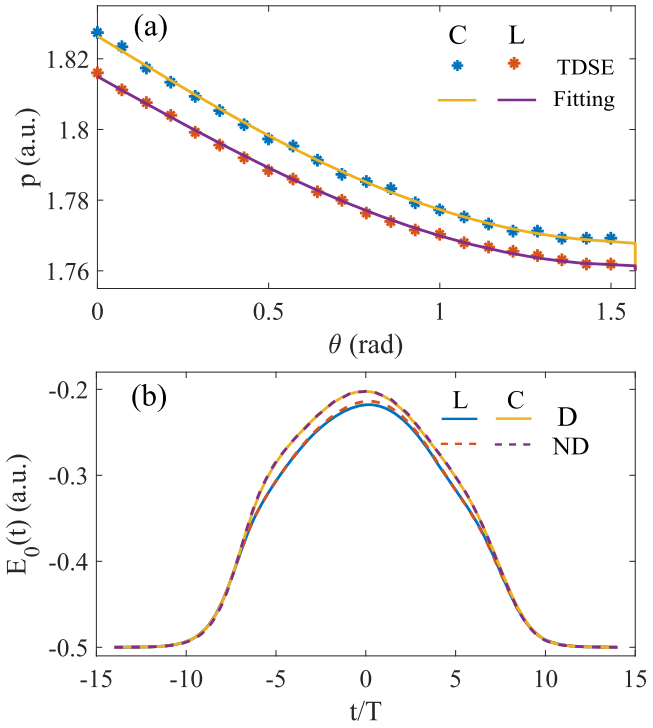

Figure 9. (a) The momentum of the interference maximum in figures 7(c) and (d). The symbols are extracted from the TDSE calculation and the solid lines are the fitting results by equation (21). (b) The time-dependent energy $E_0(t)$ of the ground state. The laser parameters are the same as those in figure 7. The solid and dashed lines are the results for the dipole and non-dipole TDSE calculation, respectively. The polarization of the laser pulses is shown in the legend.

4. Conclusion

In conclusion, we have investigated the dynamic interference of the H atom in circularly and linearly polarized pulses. The dynamic interference structures in circularly polarized pulses shift towards high energy relative to the linear case. By extracting the time-dependent energy of the ground state, we find that the AC Stark shift in circularly polarized pulses is larger than the linear case. The second-order perturbation theory and zero-order HFFT cannot fully describe the energy shift of the ground state in such an intense laser pulse, and a polynomial is raised to fit this energy shift in differently polarized pulses. This energy shift difference between the linearly and circularly polarized laser pulses leads to the interference fringe shift in the circular pulse relative to the linear case. It indicates that the experimentally available dynamic interference can be used to observe the energy difference in the ground state in linearly and circularly polarized pulses. Moreover, we demonstrate that the momentum shifts in PEMDs due to the non-dipole effect are similar for linearly and circularly polarized pulses. The AC Stark shift difference in the ground state in circularly and linearly polarized pulses is not changed by the non-dipole correction for the present laser intensities.

Acknowledgments

We thank Si-Ge Chen for useful discussion. This work was supported by the National Natural Science Foundation of China (Grant Nos. 11874163, 11804233, 11622431, 11604108 and 11627809). Numerical simulations presented in this paper were carried out using the High Performance Computing Center experimental testbed in SCTS/CGCL.

Appendix. Matrix elements of the Hamiltonian

In equation (5), we give the lowest-order non-dipole Hamiltonian. For the laser pulse polarized in the *x*-*z* plan and propagating along the positive y axis, the Hamiltonian in the spherical coordinates is written as

$$\begin{aligned} H_{\mathrm{ND}} = & -\frac{1}{2r^2}\frac{\partial}{\partial r}\left(r^2\frac{\partial}{\partial r}\right) + \frac{l(l+1)}{2r^2} - \frac{1}{r} \\ & - \frac{i}{2}\{A_z(t)[\Delta,\, r\cos\theta] + A_x(t)[\Delta,\, r\sin\theta\cos\phi]\} \\ & + \frac{r\sin\theta\sin\phi}{c}\{A_z(t)F_z(t) + A_x(t)F_x(t)\} \\ & - i\frac{r\sin\theta\sin\phi}{c}F_z(t)\frac{1}{2}[\Delta,\, r\cos\theta] \\ & - i\frac{r\sin\theta\sin\phi}{c}F_x(t)\frac{1}{2}[\Delta,\, r\sin\theta\cos\phi]. \end{aligned} \tag{A.1}$$

The first three terms are the field-free Hamiltonian of the H atom. The matrix elements of these terms in the representation of spherical harmonics are given by

$$\begin{aligned} & \langle lm|-\frac{1}{2r^2}\frac{\partial}{\partial r}\left(r^2\frac{\partial}{\partial r}\right) + \frac{l(l+1)}{2r^2} - \frac{1}{r}|l'm'\rangle\frac{R(r)}{r} \\ & = \frac{1}{r}\left(-\frac{1}{2}\frac{\partial^2}{\partial r^2} + \frac{l(l+1)}{2r^2} - \frac{1}{r}\right)\delta_{ll'}\delta_{mm'}. \end{aligned} \tag{A.2}$$

They are diagonal matrices. The forth and fifth terms are the electron–laser interaction Hamiltonian in the dipole approximation, and the matrix elements of these two terms are given by

$$\begin{aligned} & \langle lm|-\frac{i}{2}A_z(t)[\Delta,\, r\cos\theta]|l'm'\rangle\frac{R(r)}{r} \\ & = -\frac{1}{r}iA_z(t)\left[\frac{\partial}{\partial r} + \frac{-l}{r}\right]a_{l-1,m}\delta_{l-1,m}\delta_{m,m'}R(r) \\ & \quad - \frac{1}{r}iA_z(t)\left[\frac{\partial}{\partial r} + \frac{l+1}{r}\right]a_{l,m}\delta_{l+1,l'}\delta_{l+1,l'}\delta_{m,m'}R(r), \end{aligned} \tag{A.3}$$

and

$$\begin{aligned} & \langle lm|-\frac{i}{2}A_x(t)[\Delta,\, r\sin\theta\cos\phi]|l'm'\rangle\frac{R(r)}{r} \\ & = -\frac{iA_x(t)}{2r}\left[\frac{\partial}{\partial r} + \frac{l+1}{r}\right]b_{l,-m}\delta_{l+1,l'}\delta_{m-1,m'}R(r) \\ & \quad - \frac{iA_x(t)}{2r}\left[-\frac{\partial}{\partial r} + \frac{l}{r}\right]b_{l-1,m-1}\delta_{l-1,l'}\delta_{m-1,m'}R(r) \\ & \quad - \frac{iA_x(t)}{2r}\left[-\frac{\partial}{\partial r} - \frac{l+1}{r}\right]b_{l,m}\delta_{l+1,l'}\delta_{m+1,m'}R(r) \\ & \quad - \frac{iA_x(t)}{2r}\left[\frac{\partial}{\partial r} - \frac{l}{r}\right]b_{l-1,-(m+1)}\delta_{l-1,l'}\delta_{m+1,m'}R(r). \end{aligned} \tag{A.4}$$

When the laser is polarized along the $z-$axis, the magnetic quantum number m is conserved. Whereas, the component of the laser in the x axis allows the transition between the states with different magnetic quantum numbers.

The rest of the terms are the non-dipole correction of the electron–laser interaction. The matrix elements of the sixth term are given by

$$\begin{aligned} & \langle lm|\frac{r\sin\theta\sin\phi}{c}\{A_z(t)F_z(t) + A_x(t)F_x(t)\}|l'm'\rangle\frac{R(r)}{r} \\ & = \frac{A_z(t)F_z(t) + A_x(t)F_x(t)}{2cir} \\ & \quad \times (b_{l,-m}\delta_{l+1,l'}\delta_{m-1,m'} - b_{l-1,m-1}\delta_{l-1,l'}\delta_{m-1,m'} \\ & \quad + b_{l,m}\delta_{l+1,l'}\delta_{m+1,m'} - b_{l-1,-m-1}\delta_{l-1,l'}\delta_{m+1,m'})R(r). \end{aligned} \tag{A.5}$$

This term only permits the transitions between states of adjacent angular and magnetic quantum numbers. The matrix elements of the last two terms are given by

$$\begin{aligned} & \langle lm|-i\frac{r\sin\theta\sin\phi}{c}F_z(t)\frac{1}{2}[\Delta,\, r\cos\theta]|l'm'\rangle\frac{R(r)}{r} \\ & = -\frac{F_z(t)}{2cr}\Big\{-b_{l-1,m-1}a_{l-2,m-1}\left(r\frac{\partial}{\partial r} - (l-1\right) \\ & \quad \times \delta_{l-2,l'}\delta_{m-1,m'}R(r) \\ & \quad - b_{l-1,m-1}a_{l-1,m-1}\left(r\frac{\partial}{\partial r} + l\right)\delta_{l,l'}\delta_{m-1,m'}R(r) \\ & \quad + b_{l,-m}a_{l,m-1}\left(r\frac{\partial}{\partial r} - (l+1\right)\delta_{l,l'}\delta_{m-1,m'}R(r) \\ & \quad + b_{l,-m}a_{l+1,m-1}\left(r\frac{\partial}{\partial r} + (l+2\right)\delta_{l+2,l'}\delta_{m-1,m'}R(r) \\ & \quad - b_{l-1,-m-1}a_{l-2,m+1}\left(r\frac{\partial}{\partial r} - (l-1\right) \\ & \quad \times \delta_{l-2,l'}\delta_{m+1,m'}R(r) \\ & \quad - b_{l-1,-m-1}a_{l-1,m+1}\left(r\frac{\partial}{\partial r} + l\right)\delta_{l,l'}\delta_{m+1,m'}R(r) \\ & \quad + b_{l,m}a_{l,m+1}\left(r\frac{\partial}{\partial r} - (l+1\right)\delta_{l,l'}\delta_{m+1,m'}R(r) \\ & \quad + b_{l,m}a_{l+1,m+1}\left(r\frac{\partial}{\partial r} + (l+2\right)\delta_{l+2,l'}\delta_{m+1,m'}R(r)\Big\}, \end{aligned} \tag{A.6}$$

and

$$\begin{aligned} & \langle lm|-i\frac{r\sin\theta\sin\phi}{c}F_x(t)\frac{1}{2}[\Delta,\, r\sin\theta\cos\phi]|l'm'\rangle\frac{R(r)}{r} \\ & = -\frac{F_x(t)}{4cr}\Big\{-b_{l-1,m-1}b_{l-1,-(m-1)}\left(r\frac{\partial}{\partial r} + l\right) \\ & \quad \times \delta_{l,l}\delta_{m-2,m'}R(r) \\ & \quad + b_{l-1,m-1}b_{l-2,m-2}\left(r\frac{\partial}{\partial r} - (l-1\right) \\ & \quad \times \delta_{l-2,l'}\delta_{m-2,m'}R(r) \\ & \quad + b_{l-1,m-1}b_{l-1,m-1}\left(r\frac{\partial}{\partial r} + l\right)\delta_{l,l}\delta_{m,m'}R(r) \end{aligned}$$

$$
\begin{aligned}
&- b_{l-1,m-1}b_{l-2,-m}\left(r\frac{\partial}{\partial r} - (l-1)\right)\delta_{l-2,l'}\delta_{m,m'}R(r)\\
&+ b_{l,-m}b_{l+1,-(m-1)}\left(r\frac{\partial}{\partial r} + (l+2)\right)\delta_{l+2,l'}\delta_{m-2,m'}R(r)\\
&- b_{l,-m}b_{l,m-2}\left(r\frac{\partial}{\partial r} - (l+1)\right)\delta_{l,l'}\delta_{m-2,m'}R(r)\\
&- b_{l,-m}b_{l+1,m-1}\left(r\frac{\partial}{\partial r} + (l+2)\right)\delta_{l+2,l'}\delta_{m,m'}R(r)\\
&+ b_{l,-m}b_{l,-m}\left(r\frac{\partial}{\partial r} - (l+1)\right)\delta_{l,l'}\delta_{m,m'}R(r)\\
&- b_{l-1,-m-1}b_{l-1,-(m+1)}\left(r\frac{\partial}{\partial r} + l\right)\delta_{l,l}\delta_{m,m'}R(r)\\
&+ b_{l-1,-m-1}b_{l-2,m}\left(r\frac{\partial}{\partial r} - (l-1)\right)\delta_{l-2,l'}\delta_{m,m'}R(r)\\
&+ b_{l-1,-m-1}b_{l-1,m+1}\left(r\frac{\partial}{\partial r} + l\right)\delta_{l,l}\delta_{m+2,m'}R(r)\\
&- b_{l-1,-m-1}b_{l-2,-(m+2)}\left(r\frac{\partial}{\partial r} - (l-1)\right)\\
&\times \delta_{l-2,l'}\delta_{m+2,m'}R(r)\\
&- b_{l,m}b_{l+1,-(m+1)}\left(r\frac{\partial}{\partial r} + (l+2)\right)\delta_{l+2,l'}\delta_{m,m'}R(r)\\
&- b_{l,m}b_{l,m}\left(r\frac{\partial}{\partial r} - (l+1)\right)\delta_{l,l'}\delta_{m,m'}R(r)\\
&- b_{l,m}b_{l+1,m+1}\left(r\frac{\partial}{\partial r} + (l+2)\right)\delta_{l+2,l'}\delta_{m+2,m'}R(r)\\
&+ b_{l,m}b_{l,-(m+2)}\left(r\frac{\partial}{\partial r} - (l+1)\right)\delta_{l,l'}\delta_{m+2,m'}R(r)\Big\}.
\end{aligned}
\tag{A.7}
$$

Compared to other terms, these two terms not only allow the transition between adjacent angular and magnetic quantum number states but also the states differing by two quantum numbers. Moreover, the last two terms contain the operator $ri\partial/\partial r$. This operator is not Hermitian, but the following operator is Hermitian

$$
ri\frac{\partial}{\partial r} + \frac{i}{2} = \frac{1}{2}\left(ri\frac{\partial}{\partial r} + i\frac{\partial}{\partial r}r\right). \tag{A.8}
$$

In the above equations, the coefficients $a_{l,m}$ and $b_{l,m}$ are given by

$$
a_{l,m} = \sqrt{\frac{(l+1)^2 - m^2}{(2l+1)(2l+3)}}, \tag{A.9}
$$

and

$$
b_{l,m} = \sqrt{\frac{(l+m+1)(l+m+2)}{(2l+1)(2l+3)}}, \tag{A.10}
$$

respectively.

ORCID iDs

Yueming Zhou https://orcid.org/0000-0001-7772-4566

References

[1] Fuchs M *et al* 2015 Anomalous nonlinear x-ray Compton scattering *Nat. Phys.* **11** 964

[2] Stöhr J and Scherz A 2015 Creation of x-ray transparency of matter by stimulated elastic forward scattering *Phys. Rev. Lett.* **115** 107402

[3] Guetg M W, Lutman A A, Ding Y, Maxwell T J, Decker F J, Bergmann U and Huang Z 2018 Generation of high-power high-intensity short x-ray free-electron-laser pulses *Phys. Rev. Lett.* **120** 014801

[4] Lam R K *et al* 2018 Soft x-ray second harmonic generation as an interfacial probe *Phys. Rev. Lett.* **120** 023901

[5] Young L *et al* 2010 Femtosecond electronic response of atoms to ultra-intense x-rays *Nature* **466** 56

[6] McNeil B W J and Thompson N R 2010 X-ray free-electron lasers *Nat. Photonics* **4** 814

[7] Eberly J H and Kulander K C 1993 Atomic stabilization by super-intense lasers *Science* **262** 1229

[8] Gavrila M 2002 Atomic stabilization in superintense laser fields *J. Phys. B At. Mol. Opt. Phys.* **35** R147

[9] Pont M and Gavrila M 1990 Stabilization of atomic hydrogen in superintense, high-frequency laser fields of circular polarization *Phys. Rev. Lett.* **65** 2362

[10] Dörr M, Potvliege R M and Shakeshaft R 1990 Tunneling ionization of atomic hydrogen by an intense low-frequency field *Phys. Rev. Lett.* **64** 2003

[11] Su Q and Eberly J H 1990 Stabilization of a model atom in superintense field ionization *J. Opt. Soc. Am.* B **7** 564

[12] Kulander K C, Schafer K J and Krause J L 1991 Dynamic stabilization of hydrogen in an intense, high-frequency, pulsed laser field *Phys. Rev. Lett.* **66** 2601

[13] Askeland S, Sørngård S A, Pilskog I, Nepstad R and Førre M 2011 Stabilization of circular Rydberg atoms by circularly polarized infrared laser fields *Phys. Rev.* A **84** 033423

[14] deBoer M P, Hoogenraad J H, Vrijen R B, Noordam L D and Muller H G 1993 Indications of high-intensity adiabatic stabilization in neon *Phys. Rev. Lett.* **71** 3263

[15] deBoer M P, Hoogenraad J H, Vrijen R B, Constantinescu R C, Noordam L D and Muller H G 1994 Adiabatic stabilization against photoionization: an experimental study *Phys. Rev.* A **50** 4085

[16] van Druten N J, Constantinescu R C, Schins J M, Nieuwenhuize H and Muller H G 1997 Adiabatic stabilization: observation of the surviving population *Phys. Rev.* A **55** 622

[17] Liu H *et al* 2012 Low yield of near-zero-momentum electrons and partial atomic stabilization in strong-field tunneling ionization *Phys. Rev. Lett.* **109** 093001

[18] Toyota K, Tolstikhin O I, Morishita T and Watanabe S 2007 Siegert-state expansion in the Kramers-Henneberger frame: interference substructure of above-threshold ionization peaks in the stabilization regime *Phys. Rev.* A **76** 043418

[19] Toyota K 2016 Spatiotemporal interference of photoelectron wave packets and the time scale of nonadiabatic transitions in the high-frequency regime *Phys. Rev.* A **94** 043411

[20] Toyota K, Tolstikhin O I, Morishita T and Watanabe S 2008 Interference substructure of above-threshold ionization peaks in the stabilization regime *Phys. Rev.* A **78** 033432

[21] Tolstikhin O I 2008 Siegert-state expansion for nonstationary systems. IV. Three-dimensional case *Phys. Rev.* A **77** 032712

[22] Demekhin P V and Cederbaum L S 2012 Dynamic interference of photoelectrons produced by high-frequency laser pulses *Phys. Rev. Lett.* **108** 253001

[23] Demekhin P V and Cederbaum L S 2012 Coherent intense resonant laser pulses lead to interference in the time domain

seen in the spectrum of the emitted particles *Phys. Rev.* A **86** 063412
[24] Yu C, Fu N, Zhang G and Yao J 2013 Dynamic stark effect on XUV-laser-generated photoelectron spectra: numerical experiment on atomic hydrogen *Phys. Rev.* A **87** 043405
[25] Artemyev A N, Müller A D, Hochstuhl D, Cederbaum L S and Demekhin P V 2016 Dynamic interference in the photoionization of He by coherent intense high-frequency laser pulses: direct propagation of the two-electron wave packets on large spatial grids *Phys. Rev.* A **93** 043418
[26] Baghery M, Saalmann U and Rost J M 2017 Essential conditions for dynamic interference *Phys. Rev. Lett.* **118** 143202
[27] Ning Q-C, Saalmann U and Rost J M 2018 Electron dynamics driven by light-pulse derivatives *Phys. Rev. Lett.* **120** 033203
[28] Demekhin P V and Cederbaum L S 2013 Ac Stark effect in the electronic continuum and its impact on the photoionization of atoms by coherent intense short high-frequency laser pulses *Phys. Rev.* A **88** 043414
[29] Wang N and Liu A 2019 Interference effect of photoionization of hydrogen atoms by ultra-short and ultra-fast high-frequency chirped pulses *Chin. Phys.* B **28** 083403
[30] Jiang W-C and Burgdörfer J 2018 Dynamic interference as signature of atomic stabilization *Opt. Express* **26** 19921
[31] Chini M, Zhao B, Wang H, Cheng Y, Hu S X and Chang Z 2012 Subcycle ac Stark shift of helium excited states probed with isolated attosecond pulses *Phys. Rev. Lett.* **109** 073601
[32] Chu S-I and Telnov D A 2004 Beyond the Floquet theorem: generalized Floquet formalisms and quasienergy methods for atomic and molecular multiphoton processes in intense laser fields *Phys. Rep.* **390** 1
[33] Yu C and Madsen L B 2016 Sequential and nonsequential double ionization of helium by intense XUV laser pulses: revealing ac Stark shifts from joint energy spectra *Phys. Rev.* A **94** 053424
[34] Sussman B J 2011 Five ways to the nonresonant dynamic Stark effect *Am. J. Phys.* **79** 477
[35] Mi K *et al* 2020 Perturbed ac Stark effect for attosecond optical-waveform sampling *Phys. Rev. Applied* **13** 014032
[36] Reed V C and Burnett K 1991 Role of resonances and quantum-mechanical interference in the generation of above-threshold-ionization spectra *Phys. Rev.* A **43** 6217
[37] Wickenhauser M, Tong X M and Lin C D 2006 Laser-induced substructures in above-threshold-ionization spectra from intense few-cycle laser pulses *Phys. Rev.* A **73** 011401(R)
[38] Freeman R R, Bucksbaum P H, Milchberg H, Darack S, Schumacher D and Geusic M E 1987 Above-threshold ionization with subpicosecond laser pulses *Phys. Rev. Lett.* **59** 1092
[39] Jones R R 1995 Interference effects in the multiphoton ionization of sodium *Phys. Rev. Lett.* **74** 1091
[40] Korneev P A *et al* 2012 Interference carpets in above-threshold ionization: from the Coulomb-free to the Coulomb-dominated regime *Phys. Rev. Lett.* **108** 223601
[41] Tan J *et al* 2020 Resolving strong-field tunneling ionization with a temporal double-slit interferometer *Phys. Rev. A* **101** 013407
[42] Liang J *et al* 2019 Low-energy photoelectron interference structure in attosecond streaking *Opt. Express* **26** 37736
[43] Kylstra N J, Worthington R A, Patel A, Knight P L, Vázquez de Aldana J R and Roso L 2000 Breakdown of stabilization of atoms interacting with intense, high-frequency laser pulses *Phys. Rev. Lett.* **85** 1835
[44] Popov A M, Tikhonova O V and Volkova E A 2003 Strong-field atomic stabilization: numerical simulation and analytical modelling *J. Phys. B At. Mol. Opt. Phys.* **36** R125
[45] Førre M, Selstø S, Hansen J P and Madsen L B 2005 Exact nondipole Kramers-Henneberger form of the light-atom Hamiltonian: an application to atomic stabilization and photoelectron energy spectra *Phys. Rev. Lett.* **95** 043601
[46] Emelin M Y and Ryabikin M Y 2014 Atomic photoionization and dynamical stabilization with subrelativistically intense high-frequency light: magnetic-field effects revisited *Phys. Rev.* A **89** 013418
[47] Emelin M Y, Smirnov L A and Ryabikin M Y 2017 Tailoring the pulse shape to efficiently populate atomic electron metastable states in a relativistically intense high-frequency laser field *Phys. Rev.* A **96** 043420
[48] Simonsen A S and Førre M 2015 Magnetic-field-induced enhancement of atomic stabilization in intense high-frequency laser fields *Phys. Rev.* A **92** 013405
[49] Staudt A and Keitel C H 2006 Two-electron ionization and stabilization beyond the dipole approximation *Phys. Rev.* A **73** 043412
[50] Wang M-X, Liang H, Xiao X-R, Chen S-G, Jiang W-C and Peng L-Y 2018 Nondipole effects in atomic dynamic interference *Phys. Rev.* A **98** 023412
[51] Jiang W-C, Chen S-G, Peng L-Y and Burgdörfer J 2019 Two-electron interference in strong-field ionization of He by a short intense XUV laser pulse *Phys. Rev. Lett.* **124** 043203
[52] Rescigno T N and McCurdy C W 2000 Numerical grid methods for quantum-mechanical scattering problems *Phys. Rev.* A **62** 032706
[53] Jiang W-C and Tian X-Q 2017 Efficient split-Lanczos propagator for strong-field ionization of atoms *Opt. Express* **25** 26832
[54] Pont M, Walet N R, Gavrila M and McCurdy C W 1988 Dichotomy of the hydrogen atom in superintense, high-frequency laser fields *Phys. Rev. Lett.* **61** 939
[55] Pont M 1989 Atomic distortion and ac-Stark shifts of H under extreme radiation conditions *Phys. Rev.* A **40** 5659
[56] Pont M, Walet N R and Gavrila M 1990 Radiative distortion of the hydrogen atom in superintense, high-frequency fields of linear polarization *Phys. Rev.* A **41** 477
[57] Dörr R, Potvliege M, Proulx D and Shakeshaft R 1991 Multiphoton processes in an intense laser field. V. the high-frequency regime *Phys. Rev.* A **43** 3729
[58] Brennecke S and Lein M 2019 Strong-field photoelectron holography beyond the electric dipole approximation: a semiclassical analysis *Phys. Rev.* A **100** 023413
[59] Hartung A *et al* 2019 Magnetic fields alter strong-field ionization *Nat. Phys.* **15** 1222
[60] Smeenk C T L 2011 Partitioning of the linear photon momentum in multiphoton ionization *Phys. Rev. Lett.* **106** 193002
[61] Haram N *et al* 2019 Relativistic nondipole effects in strong-field atomic ionization at moderate intensities *Phys. Rev. Lett.* **123** 093201
[62] Chelkowski S, Bandrauk A D and Corkum P B 2014 Photon momentum sharing between an electron and an ion in photoionization: from one-photon (photoelectric effect) to multiphoton absorption *Phys. Rev. Lett* **113** 263005
[63] Ludwig A, Maurer J, Mayer B W, Phillips C R, Gallmann L and Keller U 2014 Breakdown of the dipole approximation in strong-field ionization *Phys. Rev. Lett.* **113** 243001